Mixing, Dispersion, and Resuspension in Vicinity of Ocean Wastewater Plume

By Libe Washburn,[1] Burton H. Jones,[2] Alan Bratkovich,[3] T. D. Dickey,[4] and Ming-Sue Chen[5]

Abstract: Buoyant plumes discharged from ocean outfalls are important for dispersing municipal wastewater into the marine environment in many coastal areas, although field studies of operating outfall systems are rare. Here, we report on an extensive field study of the effluent plume from one of the largest wastewater outfalls on the west coast of the United States. This study shows that the dispersion and mixing levels of the plume depend upon the local current speed and ambient density stratification. Under these highly stratified, late-summer conditions, we find that a combination of temperature, salinity, turbidity, and chlorophyll fluorescence measurements are required to unambiguously identify plume waters. Over the course of these observations, the local current speed at plume depth varied from 0.01 m/s to 0.07 m/s, corresponding to a Froude number Fr range of 10^{-3} to 0.2. A limited number of dilution estimates are made for the lower Fr case, and these fall in the range 110 to 160, which is within the design range for this type of diffuser. The observed maximum height of rise and wastewater field thickness are in reasonable agreement with laboratory results for zero current speed (Fr = 0). At the higher current speed, turbidity layers originating at the sea floor are observed which result from resuspension of bottom sediments.

Introduction

Municipal wastewater from heavily populated urban areas along the southern California coast is discharged into the marine environment through coastal outfalls built on the sea floor. This method of disposal is chosen because of the relatively steep bottom slope near the shore, and because the continental shelf is narrow (Gross 1983). These factors allow relatively deep discharge of effluent near the shore and provide more rapid flushing of the coastal environment by offshore waters. Effluent is injected into the ocean as a rising buoyant plume, which is rapidly diluted with ambient waters due to entrainment and mixing processes. The goal of this discharge is to reduce the environmental impact of the wastewater by achieving high levels of initial dilution. After the initial buoyant rise of effluent from an outfall system, additional mixing and dilution occur only through the action of local oceanic processes that are intermittent in space and time and are poorly understood (Csanady 1973; Koh and Brooks 1975). Several laboratory and theoretical investigations of mixing and dilution processes in buoyant plumes under idealized conditions have been conducted (Turner 1973; Morton et al. 1956; List 1982; Roberts 1977; Fischer et al. 1979; Wright 1977) and are used in the design of outfall systems. However, complexities of the coastal marine environment, e.g., variable local currents and changing ambient density stratification, are difficult to account for in theories of plume dispersal. Furthermore, differences in scale between laboratory and natural conditions make direct extrapolation of laboratory results uncertain (Fischer et al. 1979). Therefore, detailed field observations of plume structure under a variety of oceanic conditions are important for developing a more complete understanding of buoyant plume dispersal into a stratified environment.

[1]Asst. Prof., Dept. of Geography, Univ. of California, Santa Barbara, CA 93106-4060; formerly, Res. Asst. Prof., Ocean Physics Group, Dept. of Geological Sci., Univ. of Southern California, Los Angeles, CA 90089-0740.

[2]Res. Asst. Prof., Hancock Inst. for Marine Studies, Univ. of Southern California, Los Angeles, CA 90089-0371.

[3]Adjunct Prof., Dept. of Atmospheric, Oceanic, and Space Sci., Univ. of Michigan, Ann Arbor, MI 48109-2143; formerly, Ocean Physics Group, Dept. of Geological Sci., Univ. of Southern California, Los Angeles, CA 90089-0371.

[4]Prof., Ocean Physics Group, Dept. of Geological Sci., Univ. of Southern California, Los Angeles, CA 90089-0740.

[5]Field Engr., ENSECO, Garden Grove, CA 92641.

Note. Discussion open until June 1, 1992. To extend the closing date one month, a written request must be filed with the ASCE Manager of Journals. The manuscript for this paper was submitted for review and possible publication on August 31, 1989. This paper is part of the *Journal of Hydraulic Engineering*, Vol. 118, No. 1, January, 1992. ©ASCE, ISSN 0733-9429/92/0001-0038/$1.00 + $.15 per page. Paper No. 26536.

Experimental Description

We conducted an extensive field study to examine the dispersion of the effluent plume from one of the largest municipal outfall systems on the west coast of the United States. The study region (Fig. 1) lies offshore of the Palos Verdes Peninsula in southern California and contains an outfall system operated by the Sanitation Districts of Los Angeles County. This system has been the primary, single-point source for most contaminants of environmental concern in the Southern California Bight (Mearns and Young 1983).

Two shipboard surveys of the area were conducted on August 19–20, 1986, and each survey consisted of five transect lines oriented alongshore (Fig. 1). Data were collected from an instrumented platform that carries a

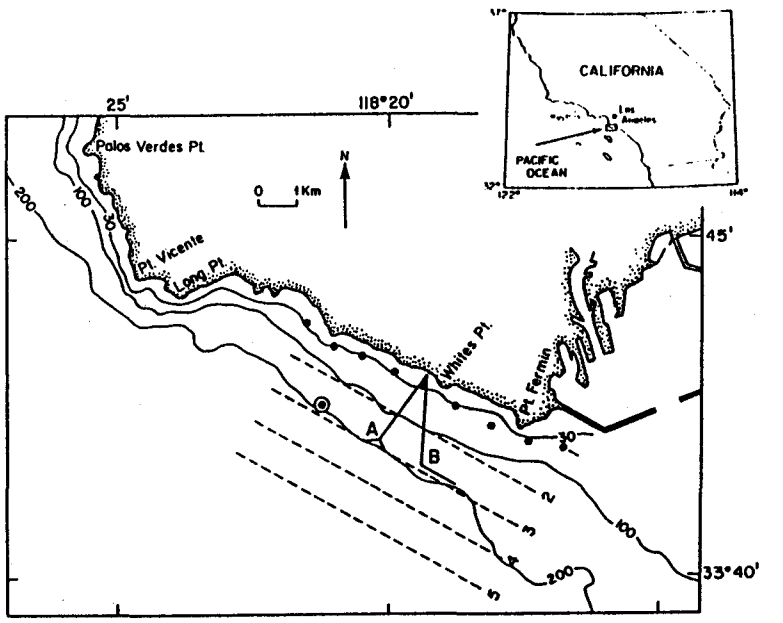

FIG. 1. Study Area Showing Two Active Outfall Diffusers, Labeled A and B; Inshore Line 1 Consists of Vertical Casts at Locations of Dots; Currents Were Measured at Location of Dot and Circle; Depth Contours in ft (1 ft = 0.305 m)

CTD (conductivity, temperature, depth instrument manufactured by Sea-Bird Electronics, Inc) and a beam transmissometer (operating with a 660-nm wavelength light source, manufactured by Sea Tech, Inc.). Initially, all signals were sampled at 33 Hz, averaged into 17 point blocks, and then stored on disk in the ship's laboratory. To stabilize estimates of salinity and density, these blocks were further averaged into half-overlapped, 10-s bins. Sampling along lines 2 to 5 (Fig. 1) was accomplished by continuously winching the platform between the surface and the bottom as the research vessel moved forward at about 1.5 m/s. Data were collected during both upcasts and downcasts to maximize horizontal resolution. This type of "tow-yo" transect provides sufficient resolution for characterizing the dispersal of the outfall plume over horizontal scales of order 500 m. To avoid damage from impacts with the bottom, an acoustic pinger is suspended just below the platform so that its position above the bottom may be determined. Generally, we estimate that data are obtained to within 5 m of the seafloor. The changes in bottom profiles between different data sections reflect the small-scale variation in seafloor topography along tracks that are nominally the same, but that may actually be displaced by several meters.

Conventional vertical profiles were collected near the shore along line 1 where tow-yo sampling was not possible due to large patches of kelp. Results presented here are mainly from two transects along line 3, which crosses very near the outfall system (Fig. 1). Only along line 3 could the plume be unambiguously identified during both surveys. Observations along the other lines are used for characterizing the properties of the surrounding water masses. We identify the two transects as Section 1, obtained from 12:22 A.M. to 1:53 A.M. Pacific Daylight Time (PDT) on August 20, 1986 and Section 2 from 5:29 A.M. to 7:09 A.M. PDT on August 19, 1986. During both these time periods, winds were very light and surface wave heights were less than 1 m.

Continuous measurements of horizontal current components and temperature were made during the observation period at three nominal depths (23, 34, and 45 m) at a shelf location approximately 2 km upcoast from the diffuser array (Fig. 1). Time series of current and temperature are shown in Fig. 2 for a 10-day period centered on the time of the towed sampling. Survey times for sections 1 and 2 are indicated by vertical dashed lines and plotted values are hourly averages (centered on the hour). In producing these plots, data were initially recorded every 4 minutes and then vector averaged (for current components) or filtered (for temperatures). Largest current speeds are greater than 0.4 m/s, and directional bias is downcoast (toward 120° true) and to a lesser extent onshore. Over this period, a transition from downcoast to upcoast flow is evident beginning on August 20 with maximum velocities at 34 m, about the depth of the effluent layer, exceeding 0.4 m/s.

A statistical summary of vector-averaged components for the 10-day period is given in Table 1. Over this time, the standard deviations of both horizontal current components exceed the mean values, and thus, the variable components dominate the current regime. This variability in the current field is probably associated with internal waves, tides, and diurnal surface wind forcing. Winant and Bratkovich (1981) and Bratkovich (1985) have examined the relationship between wind forcing and the oceanic response for southern California continental shelf waters and find high levels of variability at tidal and internal wave frequencies. Motions at these frequencies also produce corresponding temperature fluctuations.

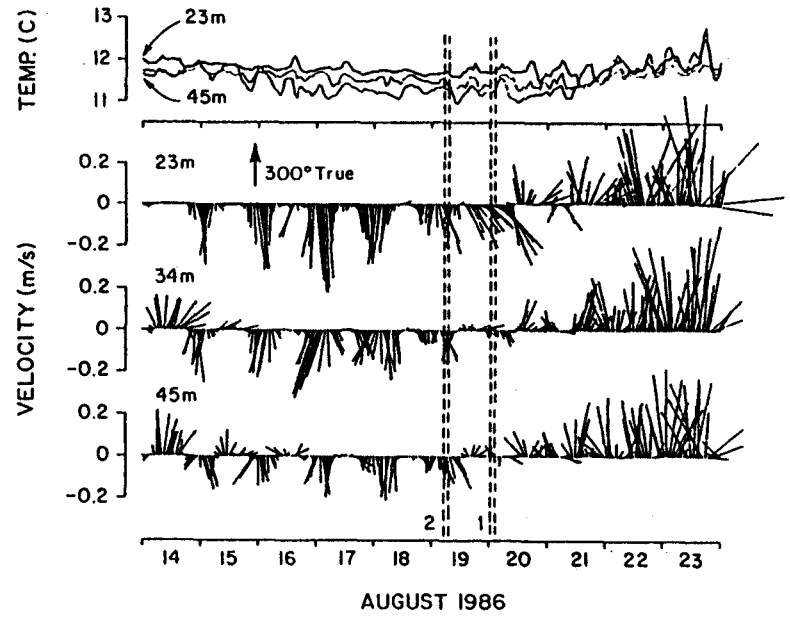

FIG. 2. Time Series of Temperature and Currents at 23, 34, and 45 m for Period August 14–23, 1986

TABLE 1. Current and Temperature Statistics (August 14–23, 1986)

Depth (m) (1)	U^a(cm/s) (2)	Average Values V^a(cm/s) (3)	T(°C) (4)	U^a(cm/s) (5)	Standard Deviation V^a(cm/s) (6)	T(°C) (7)
23	1.21	−1.10	11.82	3.24	8.58	0.14
34	0.66	0.90	11.60	2.32	7.27	0.14
45	0.16	1.30	11.49	2.22	6.06	0.33

[a]Note: Positive U is toward 30° true and positive V is toward 300° true.

Temperature stratification beneath the thermocline is moderate (0.2–0.3° C over the 11-m instrument separation), and occasional temperature inversions occur near the end of the 10-day period. Standard deviations for temperature are in the range 0.14–0.33° C (Table 1), about the same order as the average differences observed between adjacent instruments. Based on time series from the deepest instrument (45 m), temperature fluctuations tend to be enhanced near the bottom boundary, a property observed in many continental shelf environments and attributed to internal gravity wave variability [e.g., Eriksen (1982)].

Initial Plume Conditions

The effluent is injected into the water column through a pair of outfall diffusers that lie 2.5 km off the coast in a water depth of 60 m (Fig. 1). Diffuser A in Fig. 1 is 730 m long and consists of a pair of pipes, joined in

a Y, with a diameter of 2.29 m. Ports in the diffuser vary in diameter from 0.17 to 0.19 m and are spaced every 7.32 m. Diffuser B is a single pipe lying approximately alongshore. It is 1,353 m long, 3.05 m in diameter, and has ports spaced every 1.83 m, with diameters varying from 0.05 to 0.09 m. The port diameters increase toward the ends of both diffusers, which are closed. About 35% of the total volume flux passes through diffuser A in Fig. 1, while 65% passes through diffuser B. The total volume flux through the diffuser system is not constant but varies diurnally, as shown by the time series for a typical day (Fig. 3). Time series of volume flux are not available for August 19 and 20, 1986, although the total daily volume fluxes are 358 $\times 10^6$ and 366 $\times 10^6$ gal (1 gal = 3.785 $\times 10^{-3}$ m^3), respectively (Horvath 1986). In subsequent calculations, volume fluxes for the time periods of sections 1 and 2 are estimated by scaling the values of Fig. 3 by these total fluxes; the time periods of the sections are identified in Fig. 3 by vertical dotted lines labeled 1 and 2.

As the effluent emerges through the ports of the diffusers, many small buoyant plumes are formed. They rapidly coalesce and produce an effective line source of buoyancy (Koh 1982; Fischer et al. 1979). At the point of discharge, the effluent temperature T is approximately 30° C, and the salinity S is 2 practical salinity units (psu) (equivalent to parts per thousand) resulting in a density anomaly σ of -2.6 kg/m^3 (Horvath 1986; A. Steele, personal communication, 1987). Density anomaly is defined as $\sigma = \rho - 1{,}000$, where ρ = the in situ density of seawater in kg/m^3. Typical ambient seawater values for T,S, and σ at the discharge depth are 10.9° C, 33.7 psu, and 25.8 kg/m^3, respectively (Fig. 4). Therefore, the effluent is less dense than the surrounding seawater by about $\Delta\sigma$ = 28.4 kg/m^3, which results in an initial upward acceleration of the plume waters of $g' = (\Delta\rho/\rho)g$ = 0.27 m/s^2 or about 3% of g, the gravitational acceleration. About 88% of this initial density difference is due to the lower salinity of the effluent, while the small remainder results from the higher temperature. The flux of buoyancy per unit length of diffuser, or specific buoyancy flux b, defines the source strength

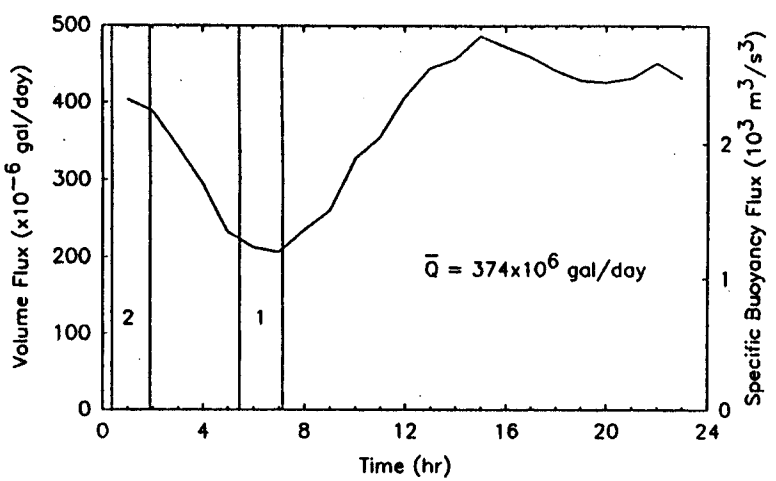

FIG. 3. Time Series of Volume Flux for Outfall System for Typical Day; Scale at Right Gives Approximate Values of Specific Buoyancy Flux; Dotted Vertical Lines Indicate Time Intervals of Data Sections

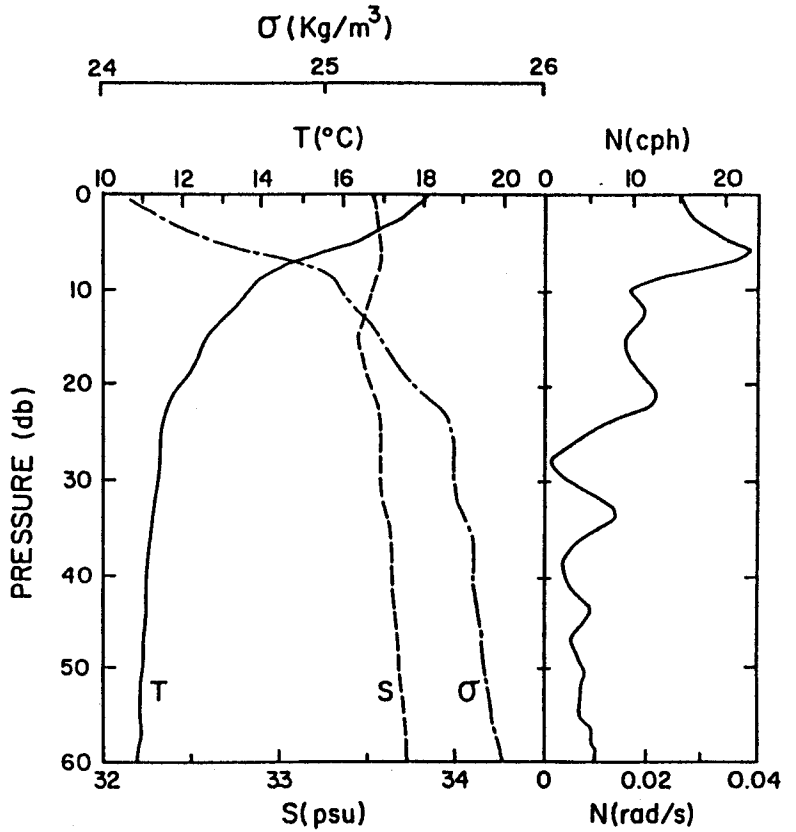

FIG. 4. Typical Background Vertical Profiles of Temperature (Solid Line), Salinity (Dashed Line), and Density Anomaly (Dash-Dot Line) in Study Area; Right Panel Shows Profile of Buoyancy Frequency

of the plume (Fischer et al. 1979) and is given by $b = g'q$, where q = the volume flux per unit length of diffuser. For both diffusers, q is approximately equal at any given time. An approximate scale for b based upon the reduced gravitational acceleration presented is shown on the right-hand scale of Fig. 3. For section 1, b is about 1.18 $\times 10^{-3}$ m^3/s^3, and for section 2, it is about 2.18 $\times 10^{-3}$ m^3/s^3, after scaling by the total daily volume fluxes.

Plume Observations

After discharge, the effluent plume rises into the water column while mixing continuously with higher density seawater. Under stratified conditions, the plume stops rising when the combined density matches the surrounding seawater density, at which point the effluent settles into a layer over the diffusers. Before settling, the mixed effluent may overshoot the equilibrium depth due to its vertical momentum. During these two surveys, the water column was well stratified, with a typical mean buoyancy frequency N defined as

$$N = \left(-\frac{g}{\rho}\frac{\partial\rho}{\partial z}\right)^{1/2} \quad \ldots\ldots (1)$$

of $1.2 \times 10^{-2}\ s^{-1}$ and a maximum of nearly $0.04\ s^{-1}$; (Fig. 4). Profiles of Fig. 4 have been scaled such that equal displacements on T and S curves indicate approximately equal changes in σ. High near-surface stratification was produced by strong summer heating of the upper 25 m. Below 25 m, both temperature and salinity gradients were stable and contributed equally to the mean background density gradient.

The simplest plume structure found during our surveys occurred when local currents were very weak. Because the effluent contains high concentrations of particles and oils relative to ambient seawater (Horvath 1986), the plume is turbid and can be observed by mapping the beam attenuation coefficient, beam c, a turbidity parameter derived from the transmissometer signal. The beam attenuation coefficient is the reciprocal of the length over which a beam of monochromatic light (660-nm wavelength in this case) has been reduced in intensity by a factor of $1/e$ due to scattering and absorption by suspended particles (Jerlov 1976; Baker and Lavelle 1984). High values of beam c, therefore, correspond to high levels of turbidity.

In section 1, the plume appears as a turbid layer, 30 m thick and 3.5 km wide, located over the diffusers at depths below 25 m [Fig. 5(*a*)]. Another layer of particles with high values of beam c is observed above 25 m, but is not due to the plume. Pumped profiles from a station between the diffusers indicate high levels of chlorophyll fluorescence in this layer, which are due to naturally occurring phytoplankton. The turbid effluent layer shows no evidence of chlorophyll. Another difference between these turbid layers is that the plume layer has high levels of ammonium (far exceeding ambient concentrations), an effluent component, while the near-surface layer does not. During the 1.5-hr period of this transect, the mean current speed (averaged between the 34-m and 45-m current meters) was very weak at about 0.01 m/s; a reliable estimate of current direction is difficult because of the very small current components. Peak values of beam c in the effluent layer exceed $1.2\ m^{-1}$, compared with surrounding values below 30 m of less than $0.6\ m^{-1}$. Two local maxima in c within the effluent layer are probably due to separate inputs from the two diffusers. Values of beam c along lines 4 and 5 (Fig. 1) are also less than $0.6\ m^{-1}$ below 30 m, indicating that the plume was shoreward of line 4 during the survey.

From the distribution of beam c in the water column [Fig. 5(*a*)], the maximum height of rise of the plume y_{max} is between 36 and 39 m, although this may be an underestimate since we cannot be certain that we observed the maximum height. For comparison with results from laboratory studies and dimensional analysis, this height may be nondimensionalized by a buoyancy length scale (Fischer et al. 1979; Roberts et al. 1989)

$$l_b = \frac{b^{1/3}}{N} \quad \ldots\ldots (2)$$

which yields the nondimensional height of rise

$$A = \frac{y_{max}}{l_b} \quad \ldots\ldots (3)$$

For these observations, $l_b = 14$ m, using b at the time of section 1 (Fig. 3) and the average buoyancy frequency between 30 m and the seafloor ($\langle N \rangle$

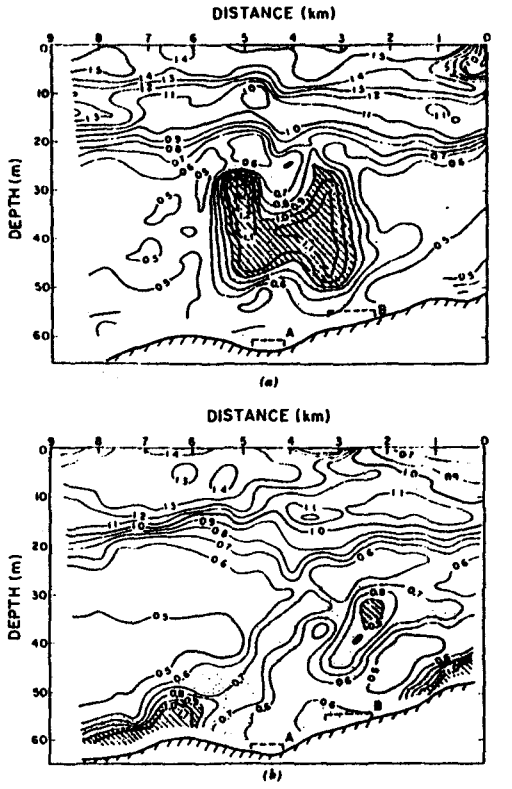

FIG. 5. Contours of Beam Attenuation Coefficient along Transect Line 3 (Fig. 1); Positions of Diffusers along Sampling Line Are Indicated with Brackets near Sea Floor, Labeled A and B; Below 25 m, Effluent Layer Is Indicated by Stippling for $c > 0.6\ m^{-1}$ and Hatching for $c > 0.9\ m^{-1}$: (*a*) Section 1; (*b*) Section 2

$= 7.6 \times 10^{-3}\ s^{-1}$). Observational estimates of A fall in the range of 2.6–2.8, using the observed range of y_{max}. These are in agreement with values of 2.84 suggested by Fischer et al. (1979) and 2.6 given by Roberts et al. (1989). These latter values of A assume that the buoyant plume rises into a motionless stratified fluid, which is approximately true for these data. Similarly, the thickness of the wastewater field h_e may also be nondimensionalized by l_b

$$B = \frac{h_e}{l_b} \quad \ldots\ldots (4)$$

and compared with analytical and laboratory results. Based on the beam c distribution, h_e ranges from 27–35 m and B ranges from 2.0–2.5. This is somewhat larger than $B = 1.8$, given by Roberts et al. (1989).

In contrast to the very weak currents of section 1, the currents were stronger during section 2, with a mean speed of 0.07 m/s directed downcoast [toward 169° true and to the right in Fig. 5(*b*)]. This higher current speed results in an effluent plume that is more dispersed and that extends beyond

the survey area along sampling line 3 [Fig. 5(*b*)]. Peak values of beam *c* above the diffusers are less than 1.0 m^{-1}, indicating lower particle concentrations (Baker and Lavelle 1984; Jerlov 1976; Spinrad 1986), and occupy a relatively small area of the section. Note that this is true despite the higher total fluxes of buoyancy and particles out of the diffusers compared with section 1. The distribution of beam *c* within the plume is less uniform on scales of order 1 km and may reflect the straining action of horizontal flow structures as they stir and distort the effluent field. Unfortunately, we are unable to estimate the nondimensional parameters *A* and *B* for this section because the effluent layer merges with the near-surface phytoplankton layer [Fig. 5(*b*)].

The effects of the plume on the temperature, salinity, and density fields are also more apparent when local currents are weak (Fig. 6) compared with when they are stronger (Fig. 7). A distinct uplifting of isotherms over the diffusers results from entrainment of colder deep water into the rising plume and is particularly evident at low current speed [Fig. 6(*a*)]. This is a consequence of the fact that the buoyancy of the plume primarily results from low salinity. Typical temperature anomalies in the plume are of the order −0.3° C, compared with the surrounding waters in the same depth range. However, temperature alone is an ambiguous indicator of the plume. The 11.2° C isotherm, which is uplifted to 35 m over the diffusers, naturally occurs at this depth between 8 and 9 km in the same section. In Fig. 6, the towpath of the instrument platform is indicated with a broken line and the end points of the profile of Fig. 4 are shown by arrows.

For both current speeds, the plume appears as a region of lower salinity with isohalines depressed downward [Figs. 6(*b*) and 7(*b*)]. The signature in density anomaly is somewhat similar, but is not as apparent [Figs. 6(*c*) and 7(*c*)]. Typical salinity anomalies in the plume are of the order −0.1 psu, and those in density are of the order 0.01 kg/m^{-3}. Because density gradients decrease with depth (Fig. 4), the spacing of isopycnal surfaces in Figs. 6(*c*) and 7(*c*) is changed by a factor of 10 below the 25.5 kg/m^{-3} surface.

Significant changes due to advection occur in the background properties throughout the water column between the times of these two sections (section 1 was obtained about 19 hr after section 2). Salinity in the upper 30 m is generally higher in section 2, with maximum near-surface salinities exceeding 33.7 psu [Fig. 7(*b*)]. Later, in section 1 they are less than 33.58 [Fig. 6(*b*)]. Also in section 2, a layer of vertically uniform salinity and temperature (at least to within 0.025 psu in salinity and 0.5° C in temperature) is found centered on 19 m from zero to six kilometers [Fig. 7(*b*)]. This layer is absent in the later section. Temporal changes in background salinity and temperature at plume depths are of the order 0.2 psu and 0.5° C, which are larger than anomalies caused by the plume itself. In bottom waters, maximum salinities in section 2 exceed 33.82 psu, and minimum temperatures are less than 10.6° C; later in section 1, maximum salinities are less than 33.72 and minimum temperatures exceed 10.8° C.

Plume Mixing and Dilution

Because of the large differences in density between the rising effluent plume and ambient ocean waters, entrainment and mixing processes are vigorous, and the properties within the plume change rapidly. The small plume-related anomalies in the local temperature, salinity, and density fields of Figs. 6 and 7 are evidence of this rapid mixing. During the buoyant rise

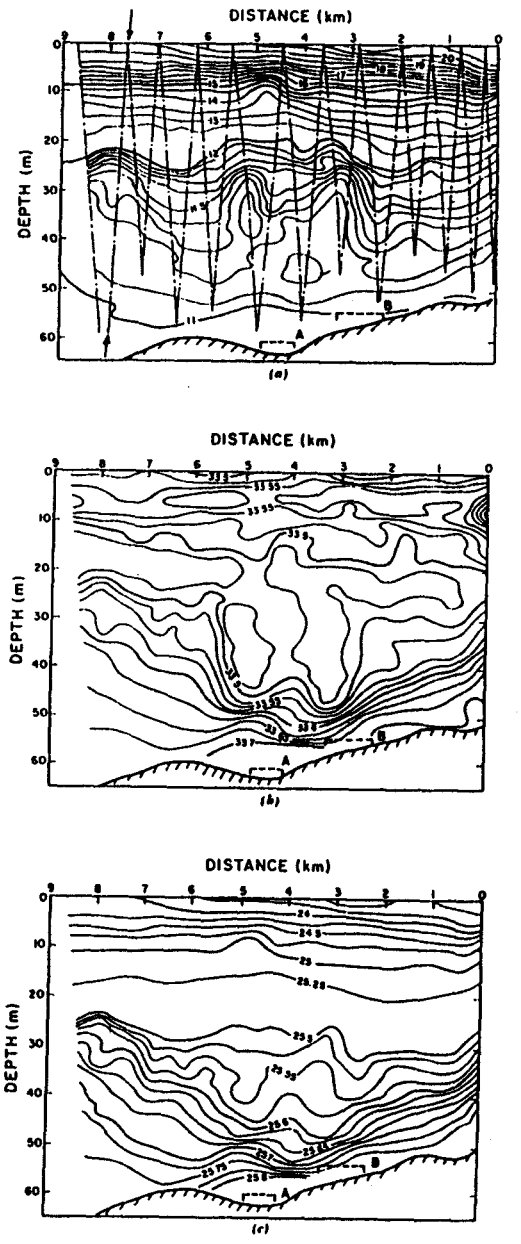

FIG. 6. Contours of Temperature for Section 1 Corresponding to Beam c Contours of Fig. 5(a). Contour Interval Varies: It is 0.5 C above 12 C isotherm and 0.1 C below; (b) Contours of Salinity for Section 1; Contour Interval is 0.025 psu Everywhere; (c) Contours for Density Anomaly; Contour Interval Varies: It is 0.25 kg/m^{-3} above 25.5 Isopyonal and 0.025 kg/m^{-3} below

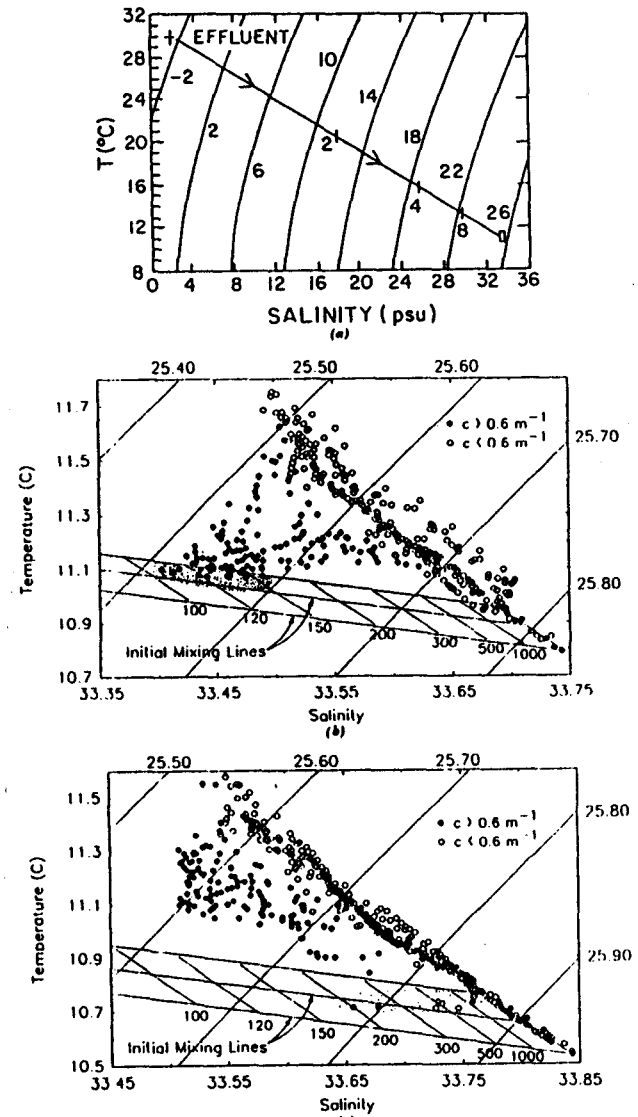

FIG. 8. (a) Large-scale *T-S* diagram [Adapted from Fischer et al. (1979)], Including Effluent Values at Upper Left End of Mixing Line and Entire Local Oceanic Range between 30 and 60 m at Lower Right End (Small Box); Arrows Indicate Direction along Initial Mixing Line and Dilutions of 2, 4, and 8 Are Shown; Lines of Constant Density Anomaly are Labeled −2 to 26; (b) Temperature-Salinity (*T-S*) Diagram for Region between 30 and 60 m along Transect Line 3 Corresponding to Figs. 5(a) and 6; Solid Circles Indicate Turbid Water with Beam c > 0.6 m⁻¹ and Open Circles Indicate Relatively Clear Water with Beam c < 0.6 m⁻¹; Lines of Constant Density Anomaly (kg/m⁻³) Slope Upward to Right and Are Labeled 25.4 to 25.8; (c) Temperature-Salinity Diagram Corresponding to Figs. 5(b) and 7; All Symbols and Parameters as in Fig. 8(b)

large. However, errors in T_B and S_B become more important with increasing D.

As effluent water parcels rise within the plume and mix with warmer and fresher ambient waters higher in the water column, their trajectories in the *T-S* plane will curve upward and away from the initial mixing lines. A schematic diagram showing this process for the case of a simple linear ambient *T-S* relation is shown in Fig. 9. A water parcel first emerges from the diffusers with effluent properties corresponding to point A at one end of the initial mixing line. The other end defining this line at B is the *T-S* point of the ambient seawater at the diffusers. The break in the line indicates that *T* and *S* at A are far from B in the diagram.

As entrainment and mixing proceed, the *T-S* point follows a curved, but unknown, trajectory to a point C, where the density of the mixed effluent equals the surrounding seawater density. Further mixing with ambient water would move point C farther along the dashed curve, while weaker mixing would leave point C back along the solid curve. Because of the complexity of turbulent entrainment and mixing processes, an essentially infinite number of trajectories are possible, which results in other mixed effluent *T-S* points such as D and E. However, all these points will be contained in the wedge-shaped region formed by the initial mixing line and the (assumed) linear, ambient *T-S* relationship. This is observed in Figs. 8(*b*) and 8(*c*), where all the *T-S* points corresponding to the effluent layer fall in the wedge-shaped region between the initial mixing lines and the approximately linear envelope of ambient *T-S* points.

Due to the variable ambient properties and the complexity of turbulent mixing processes, it is not possible, in general, to use *T* and *S* to determine the dilution field. For some points in the effluent field, however, reasonable dilution estimates can be made. This is the result of the unexpected observation that several *T-S* points lie within the families of initial mixing lines [stippled areas of Figs. 8(*b*) and 8(*c*)] and have *T-S* relationships consistent with simple end member mixing between the effluent and the deep water

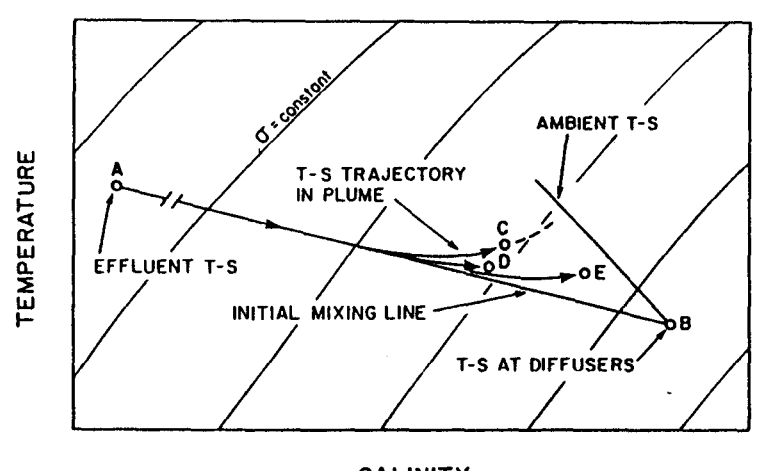

FIG. 9. Schematic Diagram Showing Trajectory in *T-S* Space of Effluent Water Parcel as It Mixes with Surrounding Ocean Waters during Plume Rise

at the diffusers, or nearly so. This is true for about 13% of the points in the plume for the case of weak currents and about 6% for the case of stronger currents. Lines of constant dilution factor D are computed by first fitting a linear regression line to background T-S points near the diffusers (to estimate values of T_B and S_B) and then evaluating (5) and (6) for these fitted points. Lines of constant D from 100 to 1,000 are shown in Figs. 8(b) and 8(c): Minimum dilutions for the case of very weak currents are mostly in the range 110–160, while at the higher current speed, where fewer points fall within the initial mixing lines, dilutions are in the range 200–600. These dilution estimates represent lower bounds, since there is some uncertainty in the actual initial mixing lines, and mixing with waters for which the T-S properties lie off the lines may have occurred.

It is also of interest to see where these points [i.e., those in the stippled regions of Figs. 8(b) and 8(c)] occur in the water column. For the case of weak currents, the points are primarily found over the diffuser labeled B at depths between 30 and 50 m [Fig. 10(a)], although a few points are found over diffuser A. For these water parcels, we hypothesize that effluent mixes with ambient waters at dilutions of 110–160 (or more) near the diffusers

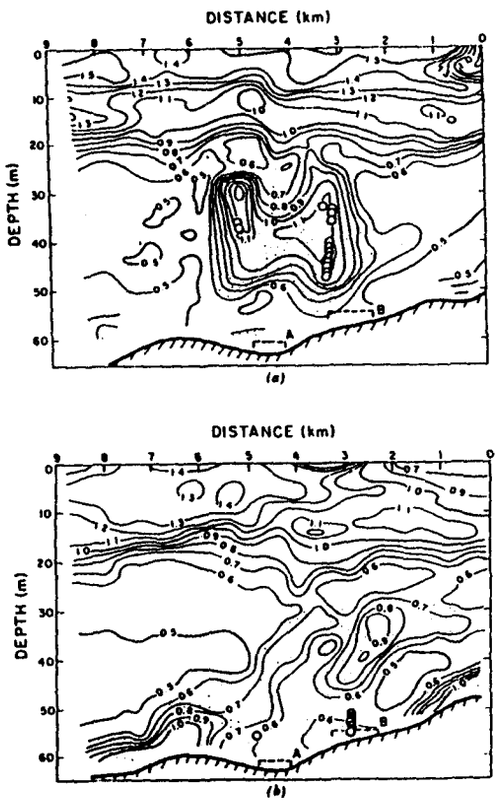

FIG. 10. (a) Location of Water Parcels Corresponding to Stippled Region in Fig. 8(b); Diffuser Locations Indicated by Brackets; (b) Location of Water Parcels Corresponding to Stippled Region in Fig. 8(c); Diffuser Locations Indicated by Brackets

and then rises in the plume with little additional mixing. If mixing higher in the water column were dominant in their formation, then they would lie well above the initial mixing lines, as is the case for all other points within the plume in Fig. 8(b). Large departures from the initial mixing lines for these latter points reflect more continuous mixing higher in the water column.

In contrast, at the higher current speed, water parcels whose T-S points fall within the stippled region of Fig. 8(c) are found only within a few meters of the diffusers [Fig. 10(b)]. This observation supports our hypothesis that points on the initial mixing lines result from mixing with ambient waters near the diffusers. The majority of mixed effluent T-S points in Fig. 8(c) lie farther from the initial mixing lines than in Fig. 8(b), a result also consistent with continuous, and perhaps more vigorous, mixing during plume rise.

Changes in plume structure and property distributions due to the increased current speed U may be parameterized by changes in the Froude number, defined as $\mathrm{Fr} = U^3/b$ (Fischer et al. 1979; Roberts 1977). This nondimensional parameter compares the competing effects of the ambient current to disperse and mix the plume (high Fr) with that of the buoyancy flux to concentrate and maintain the plume (low Fr). For these observations where both U and b change with time, Fr is 9×10^{-4} for section 1 [Fig. 5(a)] and 0.2 for section 2 [Fig. 5(b)]. The variation in Fr by a factor of about 200 may result in the striking contrast in plume structure evident between Figs. 5(a) and 5(b). Qualitatively similar changes in plume state as a function of Fr are observed in laboratory experiments at much smaller length scales (Roberts 1977). The maximum Fr expected at this site for the 10-day period around these observations is about 10^2, based on the maximum current speed of 0.5 m/s at 34 m (Fig. 2) and the minimum b of 1.18×10^{-3} m^3/s^3 (Fig. 3).

Resuspension and Dispersion of Sediments

Another effect of higher current speed is the resuspension of bottom sediments into the water column. Benthic studies in the vicinity of this outfall system suggest that previously buried outfall sediment components, such as DDT, may eventually be exposed due to resuspension processes ("Environmental" 1987). Resuspension is evident in these observations by high levels of turbidity originating at the sea floor well away from the diffusers. A cloud of high turbidity having a maximum horizontal extent of at least 3 km can be seen in Fig. 5(b) between 5 and 9 km; a second cloud is also evident between zero and 2 km. Extensive high-turbidity bottom layers are not evident for the case of weak current flow [Fig. 5(a)]. Inputs of particles from the bottom potentially complicate the interpretation of plume structure based on the distribution of beam c in the water column. However, we are able to separate the contributions to the particulate field due to effluent and bottom sediments through analysis of scatter plots of S and beam c.

In a scatter plot of beam c versus S at the low current speed, most c-S points of high turbidity ($c > 0.6$ m^{-1}) also fall within the quadrant corresponding to $S < 33.6$ psu [labeled effluent in Fig. 11(a)]. These points exhibit a linear trend and suggest a correlation between fresher and more turbid water; these water parcels are located in the effluent layer over the diffusers [open circles, Fig. 12(a)]. To test the significance of this trend, a linear regression is computed for the c-S data in the quadrant of Fig. 11(a) labeled

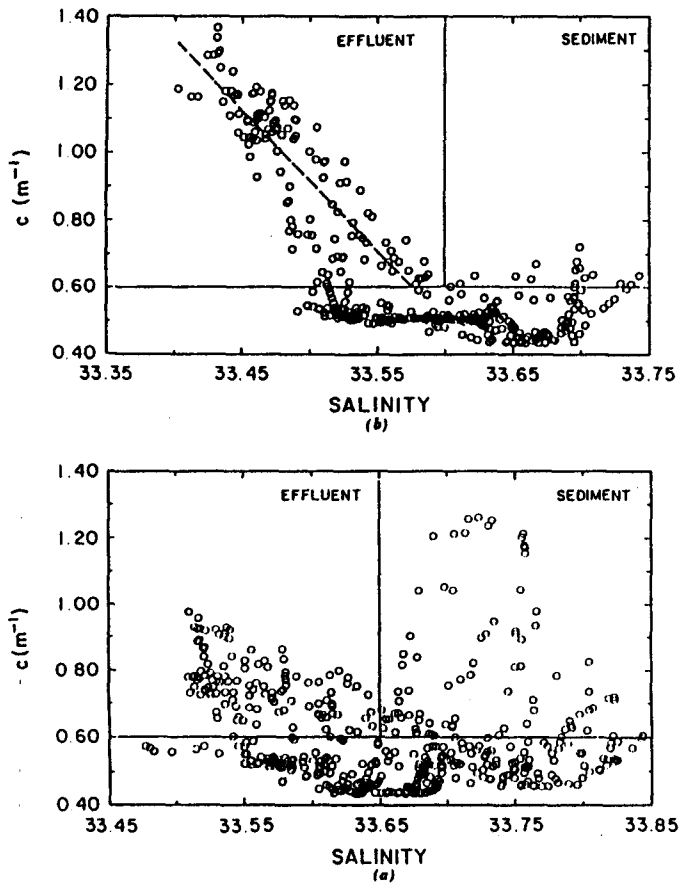

FIG. 11. (*a*) Beam Attenuation Coefficient-Salinity (*c-S*) Diagram Corresponding to Fig. 5(*a*) for Depths between 30 and 60 m; (*b*) *c-S* Diagram Corresponding to Fig. 5(*b*)

effluent. A least-squares fit to these data yields the dashed regression line with $r^2 = 0.72$ for $N = 127$. We interpret this trend as resulting from end-member mixing between the turbid, fresh effluent and clear, saline ocean waters. Scatter along the mixing line may be caused by particles settling out of the effluent layer and the fact that the ambient seawater, which mixes with the effluent, is not uniform in salinity.

At the higher current speed, *c-S* points scatter into two distinct lobes of high turbidity [$c > 0.6$ m^{-1}, Fig. 11(*b*)]. The first lobe corresponds to the effluent, as in Fig. 11(*a*), with $S < 33.65$ psu. Points in this lobe are found in the effluent layer over the diffusers [open circles, Fig. 12(*b*)], but also extend toward the southeast in the direction of current flow [to the right in Fig. 12(*b*)]. This lobe in the *c-S* diagram is compressed compared with that of Fig. 11(*a*), possibly because of increased mixing with clear, saline oceanic waters. Points in the second lobe fall in the quadrant of high salinity ($S >$ 33.65 psu) and are generally found within 15 m of the bottom [filled circles,

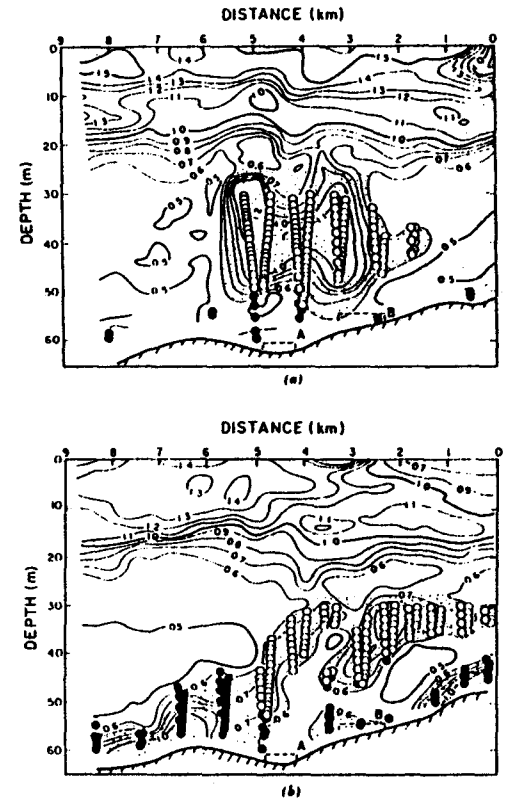

FIG. 12. (*a*) Contours of Beam Attenuation Coefficient for Same Section Shown in Fig. 5(*a*); Open Circles Give Locations of Points along Tow Path that Lie in Effluent Quadrant of Fig. 11(*a*), and Filled Circles Give Locations of Points that Lie in Sediment Quadrant of Fig. 11(*a*); (*b*) Locations of Points in Effluent Quadrant (Open Circles) and Sediment Quadrant (Filled Circles) of Fig. 11(*b*)

Fig. 12(*b*)]. The only source of this high salinity water is near the sea floor and is consistent with a sediment source of particles. A few points in the *c-S* diagram at low current speed also fall in the quandrant of high salinity of Fig. 11(*a*). These points are again found very near the sea floor [Fig. 12(*a*)] and may result from weak resuspension events. The particles that are being resuspended may be part of a thin skin of a few millimeters thickness that has been observed in the vicinity of this outfall system and has been collected in sediment traps in benthic studies (D. Weisman, personal communication, 1988).

Conclusions

This study demonstrates that ambient oceanic current and density fields have significant, quantitatively observable influences on mixing and dispersion processes in turbulent wastewater plumes. In the two sets of observations reported here, the current speed U varies from less than 0.01

m/s to about 0.07 m/s, which corresponds to a range in Froude number (Fr = U^3/b, where b = the specific buoyancy flux) of 10^{-3} to 0.2. The plume appears as a region of lower salinity, lower temperature, and increased turbidity compared to surrounding ocean waters in the same depth range. Temporal changes in temperature, salinity, and density at plume depth resulting from advection on a time scale of several hours are of the same order, or larger, than changes due to the plume itself. Salinity and the beam attenuation coefficient (beam c), a turbidity parameter, are found to be more useful than either temperature or density in observing the plume structure. However, under general oceanic conditions, we conclude that no single property is sufficient for mapping the extent of the plume, but rather distributions of all of these properties must be examined.

The water column particulate field in the vicinity of the diffusers is composed of three primary components that may be differentiated on the basis of combinations of salinity, turbidity, and chlorophyll fluorescence, at least under these observational conditions. The components are: (1) A near-surface layer of high chlorophyll fluorescence and high turbidity resulting primarily from phytoplankton; (2) a middepth layer of low salinity and high turbidity due to the effluent plume; and (3) intermittent near-bottom layers of high salinity and high turbidity that apparently result from resuspension of bottom particles.

For the higher Fr observations, beam c values are generally lower in the plume compared with those at lower Fr, which is consistent with higher dilution levels at increased current speed. This is qualitatively similar to results from laboratory and theoretical studies (Roberts et al. 1989). For the case of lower Fr, both the maximum height of plume rise and the thickness of the wastewater field are found to agree with values given by Fischer et al. (1979) and Roberts et al. (1989). A limited number of dilution estimates are made based on temperature T and salinity S, and these fall in the range from about 110 to 160 for the case of Fr = 10^{-3}. For the other case when Fr = 0.2, only a very few dilution estimates can be made, and these fall in the range 200–600. However, a systematic comparison of dilution levels versus Fr cannot be made from these estimates because sampling of the dilution field is too limited, particularly at the higher Fr. Due to the complexity of mixing and entrainment processes, we interpret these dilution estimates to be lower bounds. Outfall systems such as the one examined in this study are designed to produce average, minimum initial dilutions of order 100 (Fischer et al. 1979); (instantaneous) minimum dilutions estimated here are also of this order or larger.

The dilution estimates result from the observation that several T-S points corresponding to the plume lie along initial mixing lines which connect the T-S properties in the vicinity of the diffusers with those of the effluent at discharge. We hypothesize that these water parcels form by end-member mixing between the effluent and deeper ocean water near the diffusers and then rise in the plume with little additional mixing. Therefore, under this hypothesis, dilution estimates can be made because the mixing components are known.

This observation differs from a prediction based on dimensional analysis that the time-averaged concentrations of properties in a rising plume decrease continuously with height above the plume source (Fischer et al. 1979; Roberts 1977). However, our observations are not time averaged in the sense used in the dimensional analysis, but more nearly approximate an individual realization of a turbulent flow field. Thus, the unexpected property distributions that are observed may be a consequence of the turbulence and intermittency of mixing in this high Reynolds number plume. It should be pointed out that only a small number of T-S points are observed to lie along the initial mixing lines and that most T-S points in the plume lie well above these lines. Therefore, the properties of most mixed effluent water parcels reflect more continuous mixing with surrounding waters during plume rise.

We suggest that the observed differences in plume structure between the two sections may result from the variation in Fr by a factor of 200. However, the plume has a complex three-dimensional structure at all Fr, and we cannot be certain that other sampling sections would not yield very different distributions. Clearly, more observations of operating outfall systems are needed over a wide range of oceanic conditions to characterize the structure and turbulent entrainment processes in these plumes.

It was also found that resuspension processes are active at low to moderate current speeds at this outfall site, in the absence of strong local atmospheric forcing. While the surface wave heights were low based on visual observation, the role of surface waves in producing the observed resuspension is uncertain at this point. On longer time scales, many other processes, e.g., the seasonal modulation of density stratification and the passage of storms, are likely to be important in redistributing sediments around this outfall.

Acknowledgments

Gary S. Kleppel, David A. Siegel, and Alex Steele provided valuable assistance at sea during the experiment. We had helpful discussions with Irwin Haydock, Alex Steele, David Weisman, and Yicun Wu in the course of our analysis. Constructive criticisms of the reviewers helped improve the manuscript. This work was supported by the University of Southern California Sea Grant Program and the Sanitation Districts of Los Angeles County.

Appendix. References

Baker, E. T., and Lavelle, J. W. (1984). "The effect of particle size on the light attenuation coefficient of natural suspensions." *J. Geophys. Res.*, 89(C5), 8197–8203.

Bratkovich, A. (1985). "Aspects of the tidal variability observed on the southern California continental shelf." *J. Phys. Oceanogr.*, 15(3), 225–239.

Csanady, G. T. (1973). *Turbulent diffusion in the environment.* D. Reidel Pub. Co, Boston, Mass.

"Environmental processes affecting DDT contaminated sediments off Palos Verdes California." (1987). *Sediment Dynamics Workshop Report,* Sanitation Districts of Los Angeles County, Los Angeles, Calif.

Eriksen, C. C. (1982). "Observations of internal wave reflection off sloping bottoms." *J. Geophys. Res.*, 87(C1), 525–538.

Gross, M. G. (1983). "The coastal ocean: The regional background." *Ocean disposal of municipal wastewater,* vol. 1, Marine Resources Information Center, Mass. Inst. Tech., Cambridge, Mass., 93–128.

Fischer, H. B., List, E. J., Koh, R. C. Y., Imberger, J., and Brooks, N. H. (1979). *Mixing in inland and coastal waters.* Academic Press, New York, N.Y.

Horvath, R. W. (1986). *Monitoring report for August, 1986.* Sanitation Districts of Los Angeles County, Los Angeles, Calif.

Jerlov, N. G. (1976). *Marine optics.* Elsevier, New York, N.Y.

Koh, R. C. Y. (1983). "Delivery systems and initial dilution." *Ocean disposal of municipal wastewater*, vol. 1, Marine Resources Information Center, Mass. Inst. Tech., Cambridge, Mass., 129–175.
Koh, R. C. Y., and Brooks, N. H. (1975). "Fluid mechanics of wastewater disposal in the ocean." *Ann. Rev. Fluid Mech.*, 7, 187–211.
List, E. J. (1982). "Turbulent jets and plumes." *Ann. Rev. Fluid Mech.*, 14, 189–213.
Mearns, A. J., and Young, D. R. (1983). "Characteristics and effects of municipal wastewater discharges to the Southern California Bight, a case study," in *Ocean disposal of municipal wastewater*," vol 2, Marine Resources Information Center, Mass. Inst. Tech., Cambridge, Mass., 761–819.
Morton, B. R., Taylor, G. I., and Turner, J. S. (1956). "Turbulent gravitational convection from maintained and instantaneous sources." *Proc. Roy. Soc.*, A234, 1–23.
Roberts, P. J. W. (1977). "Dispersion of buoyant waste water discharged from outfall diffusers of finite length", thesis, presented to California Institute of Technology, at Pasadena, Calif., in partial fulfillment of the requirements for the degree of Doctor of Philosophy.
Roberts, P. J. W., Snyder, W. H., and Baumgartner, D. J. (1989). "Ocean outfalls. I: Submerged wastefield formation." *J. Hydr. Engr.*, ASCE, 115(1), 1–25.
Spinrad, R. W. (1986). "A calibration diagram of specific beam attenuation." *J. Geophys. Res.*, 91(C6), 7761–7764.
Turner, J. S. (1973). *Buoyancy effects in fluids*. Cambridge Univ. Press, Cambridge, United Kingdom.
Winant, C., and Bratkovich, A. (1981). "Temperature and currents on the southern California shelf: A description of the variability." *J. Phys. Oceanogr.*, 11(1), 71–86.
Wright, S. J. (1977). "Effects of ambient crossflows and density stratification on the characteristic behavior of round turbulent buoyant jets," thesis presented to the California Institute of Technology, at Pasadena, California, in partial fulfillment of the requirements for the degree of Doctor of Philosophy.

Study of Open-Channel Dynamics as Controlled Process

By Yuri A. Ermolin[1]

Abstract: Open-channel flow is examined as a dynamic process. Nonlinear differential equations of flow are linearized, resulting in a transfer function. The resulting function is transcendent, and convenient for use. Evaluation of a step response allows the channel-transfer function to be written simply but with a separate delay component. The function parameters depend on the distance of the channel cross section. An example of the transient response of a channel and the associated transfer function is given.

Introduction

The desire to increase efficiency of water projects leads to the development of closed-loop control systems. Examples of such projects are wastewater disposal systems of large cities (Ermolin 1990), irrigation systems in agriculture (Balogun et al. 1988), and others. One common component of such systems is the open channel; without knowledge of its dynamic characteristics it would be impossible to create closed-loop feedback control systems.

At present methods for determining open-channels dynamics are available. In the majority of cases such methods use numerical integration of continuity and momentum equations, and are characterized by complicated numerical procedures that are not always convenient for carrying out practical engineering calculations. Therefore, approximate methods deserve attention since they would allow solution of dynamic problems in analytical form with sufficient exactness. Also, there are effective methods of automatic controller synthesis in control theory that provide the required performance optimization (Solodovnikov 1967).

In this paper the writer proposes an approximate analytical solution to open-channel dynamics using transfer functions.

Theory

A prizmatic channel of constant but arbitrary cross section is examined, as shown in the Fig. 1.

Water is introduced into the channel through a control gate (location A in Fig. 1), defined as $x = 0$, where x is the distance from the gate in the direction of flow. Flow is initially uniform, such that the water flow depth (h) and velocity (v) are constant with time (t) and distance.

The St. Venant equations are frequently (Chow 1959) used to describe water flow in homogeneous prismatic open channels. One form of these equations is

[1]Asst. Prof., Automatics and Telemechanics, Moscow Inst. of Transp. Engineers, Obraztsov St., 15, 101475, Moscow, A-55, Russia, U.S.S.R.

Note. Discussion open until June 1, 1992. To extend the closing date one month, a written request must e filed with the ASCE Manager of Journals. The manuscript for this paper was submitted for review and possible publication on June 8, 1990. This paper is part of the *Journal of Hydraulic Engineering*, Vol. 118, No. 1, January, 1992. ©ASCE, ISSN 0733-9429/92/0001-0059/$1.00 + $.15 per page. Paper No. 26504.